Joint Estimation of Battery Parameters and State-of-Charge using an Extended Kalman Filter: A Single-Parameter Tuning Approach

Joint Estimation of Battery Parameters and State-of-Charge using an Extended Kalman Filter: A Single-Parameter Tuning Approach

Henrik Beelen, Henk Jan Bergveld and M.C.F. Donkers

***Abstract*—The joint estimation of the State-of-Charge and the parameters of a battery model is typically done using nonlinear extensions of the Kalman filter, such as the well-known and widely-used Extended Kalman filter (EKF), in combination with a simple but relatively accurate equivalent-circuit model. The main limitation of the joint EKF is that extensive tuning of the covariance matrices is required when implementing the observer in an application. This tuning is a tedious task with no clear guidelines for the tuning procedure. Furthermore, the joint EKF and its extensions do not explicitly address model uncertainty and sensor noise, which may be the cause for the problematic tuning. In this paper, we combine a nonlinear observer with the structured representation of model uncertainty and disturbances as typically used in a robust-observer design approach. Therefore, the joint EKF for simultaneous estimation of State-of-Charge and model parameters will be presented for the case that includes cross-correlated noises. Moreover, inspired by the conditions for enforcing convergence of the State-of-Charge estimation error, a so-called forgetting factor will be introduced to the joint EKF. These adaptations lead to an observer with a single tuning parameter. The experimental results show that tuning of the proposed observer is straightforward and that the performance is similar to a regular joint EKF with a root-mean-square State-of-Charge error of 0.5%.**

***Index Terms*—Joint Estimation, Kalman Filter, State-of-Charge Estimation, Parameter Estimation, Lithium-ion batteries**

I. Introduction

TODAY, Lithium-ion batteries are essential for enabling a technologically advanced and sustainable society. Due to the relatively high energy density, Lithium-ion batteries are used to power, e.g., a wide variety of portable devices as well as the fast-growing fleet of electric vehicles (EVs) around the world. Especially in EVs, accurate information on the remaining charge, i.e., the State-of-Charge (SoC), is of paramount importance to the driver in order to know the remaining driving range. The Battery Management System (BMS) typically monitors current, voltage and temperature, but the SoC can unfortunately not be measured directly. Therefore, the SoC is typically estimated using the measured quantities in combination with model-based techniques, see, e.g., [1, 2] and references therein. Although SoC estimation can be done with observers designed for accurate electrochemistry-based battery models, see, e.g., [3, 4], an Equivalent-Circuit Model (ECM) is often used due to its simplicity and relatively good accuracy, see, e.g., [1, 5, 6]. The ECM can be interpreted as a low-order model that approximates the dynamical behaviour of the battery voltage with linear state dynamics and a static nonlinearity in the output of the model. Due to this nonlinear relation, SoC estimation is typically done using nonlinear extensions of the Kalman filter (KF), such as the well-known and widely-used Extended Kalman filter (EKF), see, e.g., [1, 6–10].

In [6], it has been shown that the EKF, if model uncertainties are ignored and the EKF has been tuned adequately, already achieves a close-to-optimal estimation accuracy (i.e., close to the so-called Cramér-Rao lower bound). Unfortunately, the EKF (and many of its extensions) do not explicitly address the (rate of) convergence of the SoC estimation error and robustness with respect to model uncertainty and sensor noise. Namely, the estimation error of the discrete-time EKF is bounded under the conditions that the model uncertainty and disturbing noise terms are small enough, as well as that the initial estimation error is small enough, see [11]. Furthermore, sufficient conditions for local asymptotic convergence of the estimation error have been established in [12], where it has been shown that an appropriate tuning of the measurement-noise covariance matrix can significantly improve the domain of attraction. Moreover, it has been shown in [13] that the estimates of the EKF might be divergent or biased in general, whilst in [14], the EKF is found to be a good all-round choice, but not very robust against large uncertainties on the model parameters.

It has been found in [1] that in case of non-adaptive ECM parameters (i.e., the model parameters have been identified offline), the EKF fails to deliver adequate performance due to significant model inaccuracy. Namely, the model parameters typically vary due to the fact that the model is only an approximate representation of the real battery behaviour. This highlights the considerable importance of parameter adaptation to provide a more accurate model for use in real-world battery-powered applications. To realise the parameter adaptation for the adaptive EKF (e.g., joint EKF or dual EKF), additive noise is used to model the (expected) parameter variations, thereby controlling how quickly the EKF adapts the model parameters, see, e.g., [1, 8, 13]. By doing so, model uncertainty and parameter variations and its effect on the (rate of) convergence of the estimation error are considered only implicitly. Furthermore, in [1] it has been shown that, unlike the non-adaptive EKF, the joint EKF for estimation of SoC and ECM parameters requires

The authors are with the Eindhoven University of Technology, 5600 MB Eindhoven, The Netherlands (e-mail: {h.p.g.j.beelen,h.j.bergveld,m.c.f.donkers}@tue.nl). Henk Jan Bergveld is also with NXP Semiconductors, 5600 KA Eindhoven, The Netherlands.

significant tuning effort. Moreover, this tuning highly depends on the sensitivity of the model parameters with respect to the identification data. Also, in [1], it has been concluded that the EKF performance heavily depends on tuning of the covariance matrices. Typically, these matrices are tuned by trial-and-error as there are no clear guidelines for the tuning. In general, tuning is a trade-off between estimation bias and variance of the observer, as shown in [15].

In summary, the aforementioned EKF-based methods require extensive tuning of the covariance matrices, which is a tedious task without explicit tuning guidelines. To address the aforementioned drawbacks of the EKF in case of *offline* estimation of the model parameters, a robust-observer approach based on Linear Matrix Inequalities (LMIs) can be used to perform SoC estimation, see, e.g., [3, 4, 16, 17]. This approach results in observers with a structured way of capturing disturbances and model uncertainty and, consequently, tuning of the observer is likely more *straightforward*. Note that the term *straightforward* is used in the sense that (1) the number of tuning parameters is limited and (2) there are clear and explicit guidelines for tuning these parameters so that the user knows what to expect when changing a tuning parameter. However, as we will show in Section II-C, extending the robust-observer approach presented in [16], or adapting other robust-observer approaches, see, e.g., [3, 4, 17], towards joint estimation of ECM parameters and SoC is not feasible. Consequently, an observer for nonlinear systems such as the joint EKF should be considered, which suffers from non-obvious tuning as explained previously.

In this paper, an observer for nonlinear systems (i.e., the joint EKF) is combined with a structured approach of taking into account model uncertainty and disturbances. The main goal is to find an observer with straightforward tuning. More specifically, the EKF equations are rearranged to accommodate the cross-correlated disturbances that appear by assuming the aforementioned model structure. Also, a forgetting factor is introduced. The forgetting factor is inspired by the fact that the conditions for enforcing convergence of the estimation error bear a close resemblance to a so-called forgetting factor. The forgetting factor can also be interpreted as the dual of the discount factor in optimal controller design. This will lead to an adapted version of the EKF for joint estimation where the covariance matrices do not need to be chosen, or tuned, since they depend directly on the specific structure of disturbance and uncertainty. Consequently, regardless of battery model order, there is only a single tuning parameter for the observer, which allows for straightforward tuning. Note that this single-parameter tuning of the joint EKF is the main contribution of this work, since the accuracy of SoC estimation is already close-to-optimal with a perfectly tuned joint EKF [6]. The proposed observer will be validated experimentally with realistic EV drive-cycle data and compared to other existing approaches in the literature.

The outline of the paper is as follows. In Section II, the joint-estimation problem of SoC and parameter estimation with disturbances and model uncertainty will be introduced. Subsequently, in Section III, the EKF with cross-correlated noise and forgetting will be introduced in two steps. First, the EKF is extended in a generic way such that it accommodates cross-correlated noises and forgetting and, second, this extended EKF will be adapted towards the specific problem of the joint estimation of battery SoC and parameters. In Section IV, the proposed observer will be validated with realistic driving profiles of EVs obtained with an experimental setup. Furthermore, the proposed observer will be compared to other joint-estimation approaches. Section V discusses the results and, finally, conclusions will be given in Section VI.

II. State and Parameter Estimation

This section first describes the battery model including the model uncertainty and the typical disturbances in practical applications. Second, it will be shown that robust observers are not suitable for jointly estimating the SoC and the ECM parameters, motivating the need for an alternative.

A. Battery Modelling

The battery behaviour can be modelled using an equivalent circuit model (ECM), see, e.g., [1, 9], which models the battery using a static nonlinear function that describes the Electro-Motive Force (EMF) as a function of the battery SoC (i.e., EMF-SoC function) combined with a linear model (consisting of resistors and capacitors) describing the dynamic voltage behaviour, known as the overpotential. Since the battery SoC is defined as the amount of charge stored in the battery, normalised over the nominal capacity C_0, the SoC dynamics can be defined by the integral of the battery current.

In case the overpotential is assumed to be of first-order (i.e., consisting of a single RC-circuit in combination with a series resistance), the battery can be described as the following nonlinear discrete-time state-space model of the form

$$\begin{cases} \begin{bmatrix} s_{k+1} \\ o_{k+1} \end{bmatrix} &= \begin{bmatrix} 1 & 0 \\ 0 & \theta^1 \end{bmatrix} \begin{bmatrix} s_k \\ o_k \end{bmatrix} + \begin{bmatrix} \frac{T_s}{C_0} \\ \theta^2 \end{bmatrix} u_k \\ y_k &= V^{\text{EMF}}(s_k) + o_k + \theta^3 u_k, \end{cases} \tag{1}$$

in which $s_k \in [0,1]$, $o_k \in \mathbb{R}$, $u_k \in \mathbb{R}$ and $y_k \in \mathbb{R}$ denote the SoC, overpotential state, input current I_k^{batt} and output voltage V_k^{batt}, respectively, at time kT_s, in which k is the discrete time instant and T_s is the sampling time, which is $T_s = 1$s in this paper. The function $V^{\text{EMF}}(s)$ describes the nonlinear relation between the battery SoC and the EMF and this relation can be determined by performing characterisation experiments with the battery cell, which will be discussed in Section IV. The parameters $\theta = [\theta^1 \ \theta^2 \ \theta^3]^\top$, with $\theta^1 = \exp \frac{-T_s}{R_1 C_1}$, $\theta^2 = R_1(1 - \exp \frac{-T_s}{R_1 C_1})$ and $\theta^3 = R_0$, are related to the parameters of the electrical circuit elements of the ECM, see [1, 9] and references therein for more details.

The time-varying nature of the model parameters θ can be accommodated for in the model by taking the "dynamics" $\theta_{k+1} = \theta_k$, since it is assumed that the model parameters slowly vary over time and therefore $\theta_{k+1} \approx \theta_k$, see, e.g.,

[1, 8]. By extending (1) with the aforementioned model for the parameter dynamics, the battery model is then given by

$$\begin{cases} \begin{bmatrix} s_{k+1} \\ o_{k+1} \\ \theta_{k+1} \end{bmatrix} & = \begin{bmatrix} 1 & 0 & 0 \\ 0 & \theta_k^1 & 0 \\ 0 & 0 & I \end{bmatrix} \begin{bmatrix} s_k \\ o_k \\ \theta_k \end{bmatrix} + \begin{bmatrix} \frac{T_s}{C_0} \\ \theta_k^2 \\ 0 \end{bmatrix} u_k \\ y_k & = V^{\text{EMF}}(s_k) + o_k + \theta_k^3 u_k. \end{cases} \tag{2}$$

In this paper, a first-order overpotential model has been considered, as it has been shown in [5, 18] that a higher-order overpotential model not always leads to higher model accuracy. Still, the model typically does not capture all dynamics of the underlying nonlinear and infinite-dimensional physical system. This modelling mismatch can be taken into account by accommodating for the propagation of modelling errors in the model through an additive signal representing the modelling residual, which is denoted by an additive signal w_k. Moreover, in practical applications where SoC estimation is applied (e.g., in EVs), sensor noise is considered to be a well-known source of disturbance. As will be shown in Section IV.A, this disturbance can be characterised by a non-zero-mean noise signal. This noise signal might even be nonstationary, which roughly means that the (sample) bias and (sample) variance of this signal are time-varying. In the system description, noise on the current sensor can be taken into account as an additive input uncertainty on the input u_k by means of the disturbance v_k. Measurement uncertainty, i.e., an additive disturbance directly acting on the voltage output y_k, is not considered in this paper, since accurate voltage sensors can be used in practical applications, while using accurate current sensors is often more costly.

Combining the state variables s_k, o_k and θ_k into $x_k = \begin{bmatrix} s_k^\top & o_k^\top & \theta_k^\top \end{bmatrix}^\top$ and taking into account the previously defined modelling uncertainties and input disturbance, (2) can be rewritten to

$$\begin{cases} x_{k+1} & = A(\theta_k)x_k + B(\theta_k)\left(u_k + v_k\right) + E(\theta_k)w_k \\ y_k & = h(x_k) + D(\theta_k)(u_k + v_k) + F(\theta_k)w_k, \end{cases} \tag{3}$$

where $h(x_k) = V^{\text{EMF}}(s_k) + o_k$ and E and F are matrices that are used to describe the modelling residual. Measurement noise (i.e., from the voltage sensor) is not considered as v_k and w_k in (3) represent an additive input disturbance and model residual, respectively, and only act on the output through matrices D and F. For the model residual w_k, we assume that it is stationary white noise, as is often done in system identification, see, e.g., [19]. For the sensor disturbance v_k, it might be more realistic to assume that it is a bounded disturbance. Fortunately, in [16] it has been shown that observers that are optimised for (amplitude) bounded disturbances and those that are optimised for white-noise random disturbances behave almost the same. Finally, it should be noted that the nominal capacity C_0 of the battery is assumed in this paper to not change over time, since the battery experiments have been conducted in a short period of time where no significant change in nominal capacity is to be expected. However, when employing state-estimation algorithms in battery-powered applications, the battery will age over time and the capacity will fade, see [20] and references therein. In that case, C_0 should be updated, for which various methods are suggested in literature, see, e.g., [20] and references therein.

B. Structure of the Uncertainty Matrices E and F

In this paper, two types of model structures for parameter estimation of the overpotential model are considered, i.e., an Auto-Regressive model with eXogenous inputs (ARX) and an Output-Error (OE) model, which are common model structures encountered in system identification, see, e.g., [19]. We consider these model structures in this paper because of their relative simplicity. The main difference between these model structures is how they lead to a different description of the modelling residual (i.e., matrices E and F) that will be used in the EKF design. The first-order ARX model is given by

$$y_k^{\text{op}} = \frac{b_0 + b_1 q^{-1}}{1 + a_1 q^{-1}} u_k + \frac{1}{1 + a_1 q^{-1}} w_k, \tag{4}$$

where q is the shift operator (i.e., $y_{k-n}^{\text{op}} = q^{-n} y_k^{\text{op}}$) and u_k and y_k^{op} are the input and output of the overpotential model, respectively. Furthermore, a_1, b_0 and b_1 are the model parameters and the signal w_k is the modelling residual (or modelling error). A state-space realisation of (4) in observable canonical form is given by

$$\begin{cases} o_{k+1} & = \underbrace{-a_1}_{\theta_k^1} o_k + \underbrace{(b_1 - a_1 b_0)}_{\theta_k^2} u_k \underbrace{-a_1}_{\theta_k^1} w_k \\ y_k^{\text{op}} & = o_k + \underbrace{b_0}_{\theta_k^3} u_k + w_k, \end{cases} \tag{5}$$

where it can be seen clearly that the modelling residual w_k enters the state equation of the system description as $\theta_k^1 w_k$. Subsequently, for the uncertainty matrix $E(\theta)$ of the system in (3), using the overpotential model with ARX model structure in (5) yields $E(\theta) = \begin{bmatrix} 0 & \theta^1 & 0^{1\times 3} \end{bmatrix}^\top$, where, given that θ_k^1 is time-varying, $E(\theta_k)$ is time-varying as well. Note that, for compactness of notation, a matrix with zeros of size m rows and n columns is denoted by $0^{m\times n}$.

Besides the ARX model structure, a first-order OE model structure can be considered, which has the form

$$y_k^{\text{op}} = \frac{b_0 + b_1 q^{-1}}{1 + a_1 q^{-1}} u_k + w_k. \tag{6}$$

Compared to the ARX model in (4), the OE model is characterised by a different propagation of the modelling residual. Namely, if we take the coefficient $a_1 = 0$ in the second term of (4) (i.e., the propagation of w_k), we find the OE model in (6). In other words, when applying the structure of the OE model in (6) to the battery model in (3), it is found that $E(\theta) = 0^{5\times 1}$. Furthermore, it can be seen that both overpotential model structures, ARX and OE, yield $F = 1$ in (3). For more details on the ARX and OE model structures, the reader is referred to [19].

C. Robust-Observer Approaches to Joint Estimation

As mentioned previously, robust-observer approaches to battery SoC estimation have been presented in the literature,

see, e.g., [3, 4, 16]. In [3, 4], a robust observer is used in combination with electrochemistry-based battery models to estimate the SoC using estimates of the Lithium-ion concentrations. In [16], a robust observer is presented for estimating the SoC using an ECM. In general, the robust-observer approaches to battery SoC estimation can be interpreted as an alternative to the widely-used EKF. The approach presented in [16] is based on the explicit model structure in (3) with time-invariant model parameters. The main advantage of the robust-observer approach is that it addresses the convergence of the SoC estimation error and robustness with respect to model uncertainty and sensor noise explicitly, resulting in only one tuning parameter, regardless of the model order. This makes tuning of the robust observer more straightforward than tuning of the EKF, since this typically requires choosing the process-noise covariance Q and measurement-noise covariance R, which is a cumbersome task.

In case of joint estimation of states and parameters, a typical approach in the literature is to use an EKF-type of observer, such as the joint EKF, see, e.g., [1, 8]. However, based on the advantages of the robust-observer approaches as presented in [3, 4, 16] (i.e., straightforward tuning and an explicit interpretation of convergence and disturbance), a robust observer is preferred for joint estimation. To achieve this, the nonlinear system can be described as an uncertain linear system, which can be done using a polytopic system description, where the polytope is defined by a number of vertices based on the lower bounds and upper bounds of the linearised system. For example, in [17] a robust-observer approach is presented for the joint estimation of states and parameters of a time-varying system using polytopic linear models and LMIs. In order to find a robust observer gain L for the polytopic system, the LMIs need to be satisfied for every $i \in \{1, \dots, n\}$, which means that the system needs to be observable at every vertex of the polytopic system.

To assess the observability at the vertices, the nonlinear system in (3) can be denoted as

$$\begin{cases} x_{k+1} & = f(x_k, u_k) \\ y_k & = g(x_k, u_k) \end{cases} \tag{7}$$

and the observability of its linearisation can be analysed. For the sake of clarity and simplicity of this analysis, let us consider only one time-varying parameter, namely θ_k^1 in (2). However, this analysis can be easily extended to include the time-varying parameters θ_k^2 and θ_k^3 as well as higher-order overpotential models, and will lead to the same conclusion. The linearised system matrices are given by

$$\bar{A} = \frac{\partial f(x,u)}{\partial x} = \begin{bmatrix} 1 & 0 & 0 \\ 0 & \theta^1 & o \\ 0 & 0 & 1 \end{bmatrix} \tag{8a}$$

$$\bar{C} = \frac{\partial g(x,u)}{\partial x} = \begin{bmatrix} \frac{\partial V^{\text{EMF}}(s)}{\partial s} & 1 & 0 \end{bmatrix}. \tag{8b}$$

The observability matrix for this linearised system is given by

$$\mathcal{O} = \begin{bmatrix} \bar{C} \\ \bar{C}\bar{A} \\ \bar{C}\bar{A}^2 \end{bmatrix} = \begin{bmatrix} \frac{\partial V^{\text{EMF}}(s)}{\partial s} & 1 & 0 \\ \frac{\partial V^{\text{EMF}}(s)}{\partial s} & \theta^1 & o \\ \frac{\partial V^{\text{EMF}}(s)}{\partial s} & \left(\theta^1\right)^2 & o\left(\theta^1+1\right) \end{bmatrix}, \tag{9}$$

where it is found that

$$\begin{aligned} \det(\mathcal{O}) = \tfrac{\partial V^{\text{EMF}}(s)}{\partial s}\left(\theta^1 o\left(\theta^1+1\right) - o(\theta^1)^2\right) \\ - \left(\tfrac{\partial V^{\text{EMF}}(s)}{\partial s} o\left(\theta^1+1\right) - \tfrac{\partial V^{\text{EMF}}(s)}{\partial s} o\right) = 0, \end{aligned} \tag{10}$$

and, therefore, the linearised system is unobservable for every linearisation. This means that any uncertain polytopic representation of the battery system (7) will be locally unobservable, meaning that a robustly stabilising observer does not exist, or at least, cannot be synthesised using extensions of the results of [3, 4, 16] or using the approach in [17]. Consequently, a nonlinear-observer approach, based directly on the observability of the nonlinear system in (7), will be analysed next.

Instead of analysing the observability of the vertices of the linearised system (which can be used to synthesise a robust observer), let us verify whether the nonlinear system in (2) with one varying parameter (i.e., θ^1) is observable by means of using Lie derivatives, see, e.g., [1, 21] and references therein. Let $\mathrm{d}g$ denote the gradient of $g(x,u)$ given by $\mathrm{d}g = \begin{bmatrix} \frac{\partial g}{\partial s} & \frac{\partial g}{\partial o} & \frac{\partial g}{\partial \theta} \end{bmatrix}$. Then, the nth-order Lie derivative of $g(x,u)$ with respect to $f(x,u)$ is given by $L_f^n g = L_f^{n-1} L_f g$ with $L_f g = \mathrm{d}g f(x,u)$, where it should be noted that $L_f^0 g = g(x,u)$. For (7), the observability matrix is given by

$$\mathcal{O} = \begin{bmatrix} \frac{\partial g}{\partial x} \\ \frac{\partial L_f g}{\partial x} \\ \frac{\partial L_f^2 g}{\partial x} \end{bmatrix} = \begin{bmatrix} \Delta\tilde{V} & 1 & 0 \\ \Delta\tilde{V}+\Delta^2\tilde{V}\zeta & \theta^1 & o \\ \Delta\tilde{V}+3\Delta^2\tilde{V}\zeta+\Delta^3\tilde{V}\zeta^2 & (\theta^1)^2+\theta^1 & o(2\theta^1+1)+\theta^2 u \end{bmatrix}, \tag{11}$$

where $\Delta^i\tilde{V} = \frac{\partial^i V^{\text{EMF}}(s)}{\partial s^i}$ and $\zeta = s + \frac{T_s}{C_0}u$. The determinant of $\mathcal{O}$ is given by

$$\begin{aligned} \det(\mathcal{O}) = \Delta\tilde{V}\left((\theta^1)^2 o + \theta^1\theta^2 u - \theta^2 u - 2o\theta^1\right) \\ + \Delta^2\tilde{V}\big(-\theta^2 s u - 2os\theta^1 - \tfrac{T_s}{C_0}\theta^2 u^2 - 2\tfrac{T_s}{C_0} o\theta^1 u\big) \\ + \Delta^3\tilde{V}\left(os^2 + 2\tfrac{T_s}{C_0} osu + \tfrac{T_s^2}{C_0^2} ou^2\right), \end{aligned} \tag{12}$$

and the system is locally observable if $\det(\mathcal{O}) \neq 0$. Assuming that $\theta^1 \neq 0$, $\theta^2 \neq 0$ and $\frac{T_s}{C_0} \neq 0$, we have that $\det(\mathcal{O}) \neq 0$ if the system is either excited (i.e., $u \neq 0$) or not in equilibrium (i.e., $o \neq 0$) and there exist an $m \in \{1,2,3\}$ such that $\Delta^m\tilde{V} \neq 0$ (cf. [1]). Therefore, it can be stated that, generally, the nonlinear system is locally observable, meaning that it is possible to reconstruct the states of the system from input-output data. This analysis explains why nonlinear observers such as the EKF typically work very well, whereas an LMI-based robust-observer approach cannot be applied due to the

unobservable vertices of the polytopic system. Still, tuning of the nonlinear observers may be cumbersome task.

To summarise, since extending the robust-observer approaches towards joint estimation is not feasible, we propose to use a nonlinear observer — the EKF — for joint estimation. The EKF will be adapted based on the specific structure of model uncertainty and disturbance as presented in (3) so as to achieve explicit tuning with only a single tuning parameter. Although a robust version of the EKF is not uncommon, see, e.g., [22], tuning of the covariance matrices is still needed. It has been shown in [16] that the EKF yields similar performance as the robust-observer design and despite the fact that there is no robustness guarantee for the EKF, it has been shown to be stochastically stable, see, e.g., [11, 23]. Furthermore, it is widely used throughout literature for joint estimation, see, e.g., [1, 2, 8]. The systematic approach towards model uncertainty and input disturbance with the specific model structure in (3) can be achieved by including cross-correlated noises in the EKF.

To allow for parameter adaptation in case of the parameter "dynamics" $\theta_{k+1} = \theta_k$ in (2), the parameters of the (regular) joint EKF for state and parameter estimation are typically subject to additive noise. However, a physical interpretation for this cannot be given and therefore, no (artificial) additive noise is assumed for the parameters in (3). Instead, a forgetting factor can be introduced to enforce that the state and parameter estimates are based on recent data. Furthermore, the forgetting factor can be interpreted as the dual of introducing a discount factor in the cost function in optimal controller design.

Remark 1. *Under certain experimental conditions, it can happen that the system becomes unobservable, or at least poorly observable. This situation occurs when both $u_k \to 0$ and $o_k \to 0$ and might cause the SoC estimates to not converge. This problem may be solved by ensuring that the observer performs an update only if the measured data has considerable sensitivity with respect to states and parameters, see, e.g., [24].*

III. EKF WITH CROSS-CORRELATED NOISE AND FORGETTING

Since robust-observer approaches are not feasible for the joint estimation of the SoC and the ECM parameters, the joint EKF will be taken as a basis for joint estimation. This EKF will be adapted to accommodate the specific structure of uncertainty and disturbance of (3). To achieve this, the joint EKF needs to accommodate for cross-correlated noise and a forgetting factor needs to be included. As mentioned above, this forgetting factor ensures that the parameter and state estimates are only based on recent data. It should be noted that the joint EKF that is typically used for joint estimation of the SoC and the ECM parameters does neither accommodate cross-correlated noise nor includes a forgetting factor.

Fortunately, for linear systems, results for the Kalman filter (KF) exist that either consider cross-correlated noise, see, e.g., [25, Chapter 5.5], or consider a forgetting factor, see, e.g., [26, Chapter 7.4]. Even though combining these elements might be trivial, results for the KF that include both elements, to the best of our knowledge, do not exist and we will therefore develop them in this section. We will first develop the theory for linear time-varying systems and, subsequently, extend these results to an EKF form to make it suitable for jointly estimating the battery SoC and ECM parameters.

A. KF with Cross-Correlated Noise and Forgetting

First, the linear KF will be extended so as to accommodate cross-correlated noise and forgetting. Therefore, consider the linear time-varying system

$$\begin{cases} x_{k+1} &= A_k x_k + B_k u_k + \tilde{w}_k \\ y_k &= C_k x_k + D_k u_k + \tilde{v}_k, \end{cases} \tag{13}$$

where $\tilde{w}_k = G_k[w_k^\top \quad v_k^\top]^\top$ and $\tilde{v}_k = M_k[w_k^\top \quad v_k^\top]^\top$. Now, assuming that $\mathbb{E}\{w_k w_k^\top\} = 1$, $\mathbb{E}\{v_k v_k^\top\} = 1$ and $\mathbb{E}\{w_k v_k^\top\} = \mathbb{E}\{v_k w_k^\top\} = 0$, we find that

$$\mathbb{E}\left\{\begin{bmatrix}\tilde{w}_k\\ \tilde{v}_k\end{bmatrix}\begin{bmatrix}\tilde{w}_k\\ \tilde{v}_k\end{bmatrix}^\top\right\} = \begin{bmatrix}Q_k & S_k\\ S_k^\top & R_k\end{bmatrix} = \begin{bmatrix}G_k G_k^\top & G_k M_k^\top\\ M_k G_k^\top & M_k M_k^\top\end{bmatrix}, \tag{14}$$

where Q_k and R_k denote the (time-varying) process-noise covariance and measurement-noise covariance, respectively, of the noises $\tilde{w}_k$ and $\tilde{v}_k$. The cross correlation between the noises $\tilde{w}_k$ and $\tilde{v}_k$ is denoted by S_k, which is typically assumed to be $S_k = 0$ in the literature (see, e.g., [1, 8]), i.e., no cross correlation. However, in (13) and (14), S_k can be nonzero and, therefore, a formulation of the KF is required that accommodates the nonzero S_k (which can later be extended towards the nonlinear system (3)). According to [25, Chapter 5.5], the two-step KF with cross-correlated noise (i.e., $S_k \neq 0$) is given by a measurement update

$$L_k = P_k^+ C_k^\top \left(C_k P_k^+ C_k^\top + R_k\right)^{-1} \tag{15a}$$

$$\hat{x}_{k+1}^- = \hat{x}_k^+ + L_k(y_k - C_k \hat{x}_k^+ - D_k u_k) \tag{15b}$$

$$P_{k+1}^- = (I - L_k C_k)\, P_k^+ \tag{15c}$$

and the time update

$$\hat{x}_{k+1}^+ = A_k \hat{x}_{k+1}^- + B_k u_k + S_k R_k^{-1}(y_k - C_k \hat{x}_{k+1}^- - D_k u_k) \tag{15d}$$

$$P_{k+1}^+ = (A_k - S_k R_k^{-1} C_k) P_{k+1}^- (A_k - S_k R_k^{-1} C_k)^\top + Q_k - S_k R_k^{-1} S_k^\top, \tag{15e}$$

where taking $S_k = 0$ will yield the regular KF.

Subsequently, to fully implement the structure of the robust observer in the EKF structure, "forgetting" is necessary to allow for parameter adaptation since it is assumed in (2) that $\theta_{k+1} = \theta_k$, i.e., no parameter adaptation[1]. To allow for the "forgetting", a forgetting factor γ can be implemented, which is often used in estimation schemes, i.e., new data (or new observations) are considered to be (exponentially) more important than older data.

[1]It should be noted that this is a different approach than the approach for parameter adaptation with the (regular) joint EKF. Namely, in that case, the parameters are subject to additive noise, i.e., $\theta_{k+1} = \theta_k + r_k$, where the noise r_k is zero-mean and white with a Gaussian distribution. The variance of r_k is taken as a tuning parameter so as to achieve the desired performance for the parameter adaptation. As mentioned previously, tuning of this variance may be a tedious task and, therefore, using a forgetting factor (with straightforward tuning) can be interpreted as an alternative for the additive noise.

An implementation of this forgetting or "fading memory" is presented in [26, Chapter 7.4]. Using this approach as a starting point, a forgetting factor γ is added to (15). The implementation of this forgetting factor is given in the Appendix. The resulting two-step KF with cross-correlated noise and forgetting is given by the measurement update

$$L_k = \tilde{P}_k^+ C_k^\top (C_k \tilde{P}_k^+ C_k^\top + \gamma R_k)^{-1} \tag{16a}$$
$$\hat{x}_{k+1}^- = \hat{x}_k^+ + L_k(y_k - C_k \hat{x}_k^+ - D_k u_k) \tag{16b}$$
$$\tilde{P}_{k+1}^- = \tfrac{1}{\gamma}(I - L_k C_k)\tilde{P}_k^+ \tag{16c}$$

and the time update

$$\hat{x}_{k+1}^+ = A_k \hat{x}_{k+1}^- + B_k u_k + S_k R_k^{-1}(y_k - C_k \hat{x}_{k+1}^- - D_k u_k) \tag{16d}$$
$$\tilde{P}_{k+1}^+ = (A_k - S_k R_k^{-1} C_k)\tilde{P}_{k+1}^- (A_k - S_k R_k^{-1} C_k)^\top + Q_k - S_k R_k^{-1} S_k^\top, \tag{16e}$$

where $\gamma \leq 1$ is the forgetting factor[2], which is typically chosen close to 1, e.g., $\gamma = 0.999$. This adapted KF formulation can now be applied to the LTI system in (13). However, in order to apply the KF with cross-correlated noise and forgetting (16) to the nonlinear battery system in (3), it is necessary to extend the formulation in (16) towards an EKF formulation, which will be given in the following subsection.

B. EKF for Battery Joint Estimation

In order to apply the newly derived KF with correlated noise and forgetting[3] in (16) to the nonlinear system in (3) so as to perform joint estimation of battery states and parameters, a nonlinear extension of the KF is needed. First, the system in (3) is rewritten to

$$\begin{cases} x_{k+1} &= \underbrace{A(\theta_k)x_k + B(\theta_k)u_k}_{=f(x_k,u_k)} + G(\theta_k) r_k \\ y_k &= \underbrace{h(x_k) + D(\theta_k)u_k}_{=g(x_k,u_k)} + M(\theta_k) r_k, \end{cases} \tag{17}$$

where $r_k = [w_k^\top \quad v_k^\top]^\top$. The system in (17) is nonlinear due to the function $h(x_k)$ in the output equation and, besides the parameter-dependent matrices $A(\theta)$, $B(\theta)$ and $D(\theta)$, the matrices $G(\theta) = [E(\theta) \quad B(\theta)]$ and $M(\theta) = [F \quad D(\theta)]$ are also parameter-dependent. Second, recall that the state vector is given by $x_k = [s_k^\top \quad o_k^\top \quad \theta_k^\top]^\top$, i.e., the state vector is augmented with the parameter vector. Subsequently, in order to obtain an EKF implementation, the state equations are linearised at each time instant k, see, e.g., [8]. Consequently, the linearised system matrices A_k and C_k of are given by

$$A_k = \tfrac{\partial f(x_k,u_k)}{\partial x_k} = \left[\begin{array}{cc|ccc} 1 & 0 & 0 & 0 & 0 \\ 0 & \theta_k^1 & o_k & u_k & 0 \\ \hline 0 & 0 & 1 & 0 & 0 \\ 0 & 0 & 0 & 1 & 0 \\ 0 & 0 & 0 & 0 & 1 \end{array}\right] \tag{18}$$

and

$$C_k = \tfrac{\partial g(x_k,u_k)}{\partial x_k} = \left[\begin{array}{c|cccc} \tfrac{\partial V^{\mathrm{EMF}}(s_k)}{\partial s_k} & 1 & 0 & 0 & u_k \end{array}\right]. \tag{19}$$

Now, the EKF for joint estimation with the specific structure for model uncertainty and input disturbance as in (3) is found by using the linearised system matrices A_k and C_k, as in (18), in the KF equations in (16). An important property of the resulting algorithm and a valuable contribution of this work is that there is only one tuning parameter: the forgetting factor γ. The tuning procedure of γ is relatively easy: start with $\gamma = 1$, which can be interpreted as "no forgetting" (i.e., the EKF with correlated noise) and gradually decrease γ until the algorithm yields satisfactory performance (in terms of the estimation error). Results of the procedure with an experimental setup will be presented in Section IV.

In order to apply the EKF in (16) to the battery system (17), the remaining matrices B_k, D_k and the covariance matrices Q_k, R_k and S_k in (16) need to be known. The matrices $B_k = B(\theta_k)$ and $D_k = D(\theta_k)$ can be taken directly from (17). The covariance matrices have been defined in (14) for system (13) and we can obtain them for system (17) by taking $Q_k = G(\theta_k)G(\theta_k)^\top$, $R_k = M(\theta_k)M(\theta_k)^\top$ and $S_k = G(\theta_k)M(\theta_k)^\top$. Finally, as mentioned in Section II-B, the matrices $E(\theta_k)$ and F, which appear in $G(\theta_k)$ and $M(\theta_k)$, depend on the chosen model structure for the battery model, which implies that Q_k, R_k and S_k depend on the model structure. Namely, if an ARX model structure is chosen, then

$$\bar{G}(\theta) = \begin{bmatrix} 0 & \frac{1}{C_0} \\ \theta^1 & \theta^2 \end{bmatrix} \quad \text{and} \quad M(\theta) = \begin{bmatrix} 1 & \theta^3 \end{bmatrix}, \tag{20}$$

where for compactness of notation $\bar{G}(\theta)$ is used, since $G(\theta) = \begin{bmatrix} \bar{G}^\top(\theta) & 0^{2\times 3} \end{bmatrix}^\top$. Consequently, $\bar{Q}_k = \bar{G}(\theta_k)\bar{G}^\top(\theta_k)$ and

$$Q_k = \begin{bmatrix} \bar{Q}_k & 0^{2\times 3} \\ 0^{3\times 2} & 0^{3\times 3} \end{bmatrix}. \tag{21}$$

Using the ARX-model structure yields

$$\bar{Q}_k = \begin{bmatrix} \frac{1}{C_0^2} & \frac{\theta_k^2}{C_0} \\ \frac{\theta_k^2}{C_0} & (\theta_k^1)^2 + (\theta_k^2)^2 \end{bmatrix}, \; S_k = \begin{bmatrix} \frac{\theta_k^3}{C_0} \\ \theta_k^1 + \theta_k^2 \theta_k^3 \\ 0^{3\times 1} \end{bmatrix}, \; R_k = 1 + (\theta_k^3)^2. \tag{22}$$

In case of an OE model, $\bar{G}(\theta)$ and $M(\theta)$ are given by

$$\bar{G}(\theta) = \begin{bmatrix} 0 & \frac{1}{C_0} \\ 0 & \theta^2 \end{bmatrix} \quad \text{and} \quad M(\theta) = \begin{bmatrix} 1 & \theta^3 \end{bmatrix}, \tag{23}$$

leading to

$$\bar{Q}_k = \begin{bmatrix} \frac{1}{C_0^2} & \frac{\theta_k^2}{C_0} \\ \frac{\theta_k^2}{C_0} & (\theta_k^2)^2 \end{bmatrix}, \quad S_k = \begin{bmatrix} \frac{\theta_k^3}{C_0} \\ \theta_k^2 \theta_k^3 \\ 0^{3\times 1} \end{bmatrix}, \quad R_k = 1 + (\theta_k^3)^2. \tag{24}$$

Based on the two model structures considered in Section II-B, two different sets of the covariance matrices $\bar{Q}_k$, R_k and S_k are presented in (22) and (24). It can be seen that the covariance matrices based on the ARX model in (22) differ from the covariance matrices based on the OE

[2] It should be noted that [26] defines the forgetting factor as the reciprocal of the notation used in this paper, meaning that the forgetting factor is $\gamma \geq 1$ in [26]. We use this notation as it makes the forgetting factor to have a similar interpretation as the forgetting factor typically used in Recursive Least Squares (RLS).

[3] Recall that the KF with correlated noise (i.e., $S_k \neq 0$) may be interpreted as the standard or fully-fledged KF. Still, to emphasise that $S_k \neq 0$, we use the term "KF with correlated noise".

model in (24), except for R_k. For instance, note the missing $(\theta_k^1)^2$ and θ_k^1 terms in $\bar{Q}_k$ and S_k, respectively, for the OE model in (24) compared to the ARX model in (22). As a result, the assumed variance on the second state of the system (i.e., the overpotential state o_k) is substantially smaller for the OE case than in the ARX case since typically $\theta_k^1 \lessapprox 1$ and θ_k^2 is relatively small. Therefore, similar to a regular (joint) EKF, choice of model structure and model order (of the overpotential model) mainly depends on, first, model quality (i.e., modelling accuracy in terms of open-loop simulation) and, second, trial and error with the proposed algorithm and the resulting estimation accuracy.

To summarise, an EKF for battery joint estimation has been constructed with only one tuning parameter and two pre-tuning choices, namely, model structure and model order of the overpotential model. For brevity, we will refer to the proposed joint EKF with Correlated noise and Forgetting as "joint EKF CF". Note that, in contradiction to typical implementations of the EKF for joint estimation, the matrices Q_k, R_k and S_k are time-varying in the proposed algorithm, which is due to the specific uncertainty structure used in the system in (3). The computational complexity of the proposed EKF is not significantly larger than that of existing EKF methods.

IV. Results

In this section, the tuning and performance of the proposed observer will be evaluated and compared to existing observers using realistic EV drive-cycle data. First, the experimental setup and the two experimental drive cycles will be discussed. Second, the effects of design choices (i.e., tuning and model structure) for the proposed joint EKF CF will be analysed and, finally, the joint EKF CF will be compared to other existing model-based estimation methods, using the experimental drive cycles.

A. Experimental Setup and Test Profiles

To extensively validate the proposed observer, an experimental setup has been used which is controlled by a LabVIEW interface and consists of a climate chamber, an electronic load and power supply and two current sensors. The first current sensor is a highly accurate laboratory-grade (lab-grade) sensor (LEM IT 60-S ULTRASTAB) and is used for battery characterisation, e.g., obtaining an EMF-SoC curve and identification of a battery model with time-invariant parameters. This lab-grade current sensor is also used to generate a reference for SoC estimation by integrating the current measurements, i.e., using the so-called Coulomb-Counting (CC) method, to obtain the true SoC, see, e.g., [27]. The second current sensor is a production-grade sensor (LEM DHAB S/133), which is typically used for automotive applications (e.g., EVs) and is used for validating the observers. The current measurements obtained using the two sensors will be compared below. The battery cell under test is a Lithium Nickel Cobalt Aluminium Oxide ($LiCoNAlO_2$) cell with a (measured) nominal capacity of $C_0 = 12.6$Ah and a nominal voltage of 3.68V. The EMF-SoC curve, i.e., the function $V^{\text{EMF}}(s)$ in (2), is shown in Fig. 1

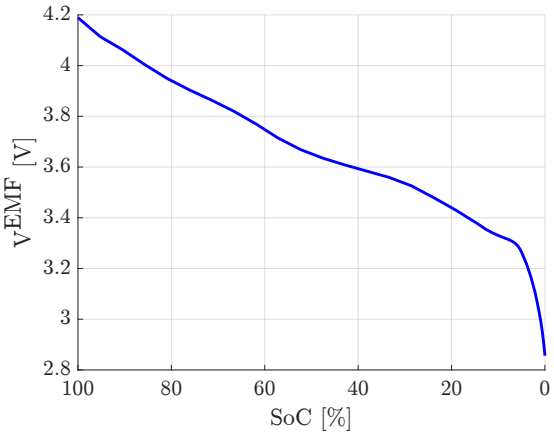

Fig. 1: EMF-SoC curve.

and is characterised with a pulsed-current test using data from the lab-grade current sensor.

In order to test the proposed observer and to compare the observer to existing approaches, the battery needs to be excited with a certain current profile. In this paper, a test case has been created that is as close to a real application as possible. Therefore, the test profiles are based on an EV application where a vehicle speed profile is taken in combination with a model of the longitudinal vehicle dynamics to obtain a current profile for the battery pack of the vehicle. It should be noted that highly dynamical current profiles have been used, which avoids potential issues with observability (cf. Remark 1). Subsequently, assuming a certain capacity of the battery pack in combination with a typical nominal pack voltage of 400 V, and an efficiency of the regenerative braking of $\eta_r = 0.6$, the current for one battery cell is obtained. Subsequently, this current has been used to excite the battery. All tests have been conducted in the climate chamber at a temperature of $20°$C.

The velocity profiles selected for the experiment are the class-3 cycle of the Worldwide harmonized Light vehicles Test Procedure (WLTP) and a number of velocity profiles that were measured on the road in the Netherlands, with both city and highway driving. Using these velocity profiles, two experimental drive cycles have been constructed with the aim of achieving a significant discharge of the battery in order to test the observers in a substantial part of the SoC range. Therefore, the first drive cycle consists of a repetition of six WLTP cycles on a 40-kWh battery pack as shown in the left column of Fig. 2, where the battery is discharged from SoC $= 97\%$ to SoC $= 28\%$. In Fig. 2a, the velocity profile of the drive cycle is shown and in Fig. 2c and Fig. 2e, the measured battery current (using the production-grade sensor) and battery voltage, respectively, are depicted.

The second drive cycle is the MMD cycle[4] and is shown in the right column of Fig. 2 and consists of three trips of city and highway driving on a single charge of a 80-kWh

[4]The MMD cycle consists of three separate trips starting in Eindhoven and ending in different places in the Netherlands, combined in one cycle with a total length of 232km. Trip 1: Eindhoven to Mijdrecht (M), 119km. Trip 2: Eindhoven to Meterik (M), 51km. Trip 3: Eindhoven to Demen (D), 62km. All trips consist of both highway and city driving.

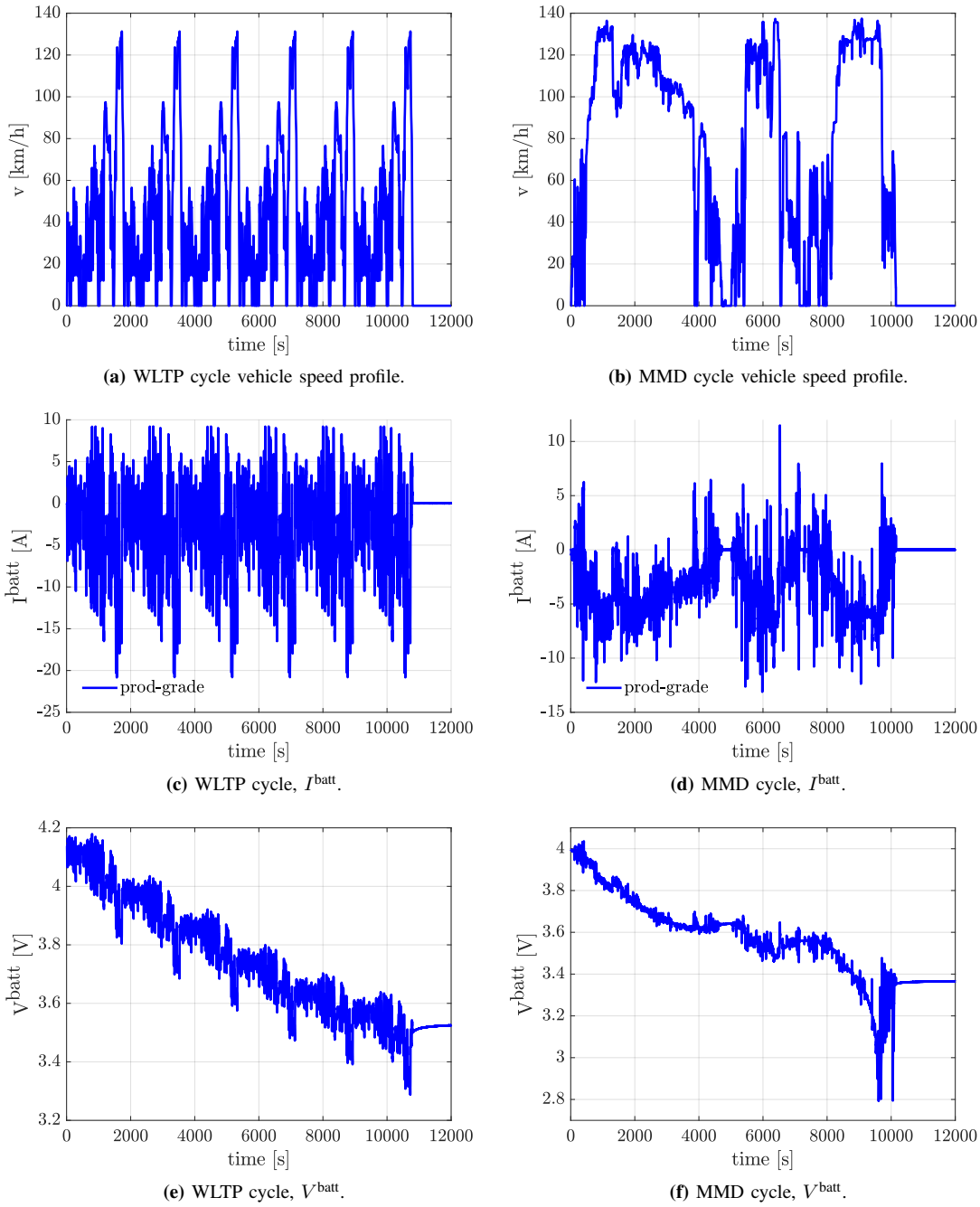

(a) WLTP cycle vehicle speed profile.

(b) MMD cycle vehicle speed profile.

(c) WLTP cycle, I^{batt}.

(d) MMD cycle, I^{batt}.

(e) WLTP cycle, V^{batt}.

(f) MMD cycle, V^{batt}.

Fig. 2: Experimental EV drive cycles.

battery pack, where the battery is discharged from SoC $= 85\%$ to SoC $= 14\%$. Observe the changing voltage behaviour at the end of the MMD cycle in Fig. 2f, after approximately $t = 9000$s, where the SoC is dropping below 20%. This behaviour indicates a slower rate of diffusion, implying that the model parameters have changed, i.e., larger internal resistance causing a larger overpotential and thus a larger voltage drop as observed in Fig. 2f. In other words, the battery behaviour becomes more nonlinear, which clearly motivates the necessity of estimating model parameters online as opposed to offline estimation, which will be further substantiated through the results in this section.

Lastly, comparing the measurements of the lab-grade current sensor with the production-grade current sensor motivates the need for SoC estimation in general. In Fig. 3, a short section of the measured current with the production-grade sensor from Fig. 2c is shown, which now also includes the data from the lab-grade current sensor. It can be seen that the production-grade sensor in blue is biased and can be characterised by a significantly higher standard deviation than the lab-grade current sensor. Moreover, this bias is time-varying (i.e., sensor drift) and is therefore calculated as the absolute average of the

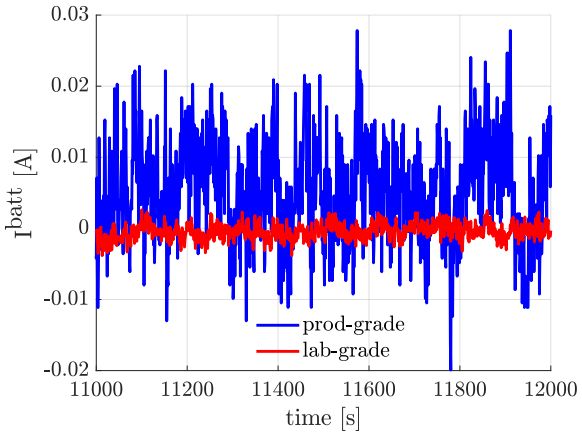

Fig. 3: WLTP cycle, zoom of I^{batt} with production-grade sensor (blue) and lab-grade sensor (red).

difference between the two current signals, which is found to be 26 mA for the WLTP drive cycle and 33 mA over the MMD cycle. Although this might seem small, a bias of 33 mA over a time of 4 hours will result in an SoC error of 1.3% using the production-grade sensor in combination with the CC method for the battery cell used in this paper.

B. Results of EKF with Correlated Noise and Forgetting

As mentioned in Section III, the joint EKF CF is characterised by only one tuning parameter, i.e., γ, and two pre-tuning choices, i.e., model structure and model order of the overpotential model. In this paper, a first-order model is chosen as denoted in (4) and (6) for the ARX model and OE model, respectively. Consequently, observer synthesis of the joint EKF CF depends on γ and the choice for either an OE or ARX model structure. The effect of these choices is analysed by synthesising different observers for these different choices and applying the observers to the measured WLTP data in Fig. 2. In order to verify convergence of the estimation error and thus the effect of γ, the initial conditions are taken as SoC $= 92\%$ (i.e., 5% deviation with respect to the true SoC) and $\theta_0^1 = 0.95$, $\theta_0^2 = 0$ and $\theta_0^3 = 0.01$. It should be noted that the initial parameter values θ_0 are taken close to the parameter values that have been found through offline characterisation of the parameters using the WLTP cycle. Furthermore, recall that the measured current used for estimation is taken from the less-accurate production-grade sensor in Fig. 2c.

The results of this study in terms of parameter estimation and SoC estimation are shown in Fig. 4. In this figure, the left column depicts the results for an ARX model structure and the right column depicts the results for an OE model structure. The estimates of the parameters θ_k^1, θ_k^2 and θ_k^3 and the SoC estimation error are depicted from top to bottom, respectively. For every plot with parameter estimates, the dashed black line shows the parameter values that have been estimated offline and the coloured dashed lines depict the estimated parameters using the joint EKF CF for a range of γ values. The offline identification of the battery model was performed by taking a different section of the WLTP data such that the validation data do not overlap entirely with the identification data. Moreover, the black dashed lines show that there is a significant difference between the offline parameters of the OE model and the ARX model. For the online estimation with the joint EKF CF, it can be seen from the plots in Fig. 4 that decreasing γ results in more "aggressive" adaptation of the parameter, which can be explained by the fact that a smaller γ results in faster "forgetting" of older data and thus faster adaptation. Interestingly, in case of an ARX model structure, θ_k^1 and θ_k^2 do not seem to converge to the offline parameters for the selected initial conditions for the state and parameter estimates, whereas for the OE model structure, θ_k^1 and θ_k^2 converge more closely to the offline parameter values (i.e., the dashed black line). It seems that using the ARX model structure in the (nonconvex) joint estimation problem is more sensitive for initial conditions than the OE model structure.

In Fig. 4g and Fig. 4h, the SoC estimation errors are shown for the ARX model structure and OE model structure, respectively. Similar to the parameter-estimation results, it can be seen that decreasing γ results in faster and more "aggressive" adaptation. Moreover, it can be seen that the SoC error in Fig. 4h with the OE model structure is significantly smaller than the SoC error in Fig. 4g using the ARX model structure for the selected initial conditions for the state and parameter estimates. This might again be due to the fact that the ARX model structure is more sensitive for initial conditions than the OE model structure. Therefore, we will take the OE model structure for the joint EKF CF and subsequently, only γ is a tuning parameter for the algorithm, where, based on the results with WLTP data in Fig. 4, $0.999 \leq \gamma \leq 0.9999$ is preferred.

C. Comparison with Existing Approaches

The proposed joint EKF CF will be compared to existing model-based estimation methods, using the model in (2). First, the need for online estimation of parameters will be shown. Second, it will be shown that the estimation accuracy of the joint EKF CF, which has only one tuning parameter, is comparable to other state-of-the-art estimation techniques, which typically have a multitude of tuning parameters. The latter will demonstrate the main contribution of this work: an accurate joint-estimation method with only a single tuning parameter γ with straightforward tuning.

For the comparison, a number of commonly-used estimation methods are selected. First, to show the necessity of online parameter estimation, the proposed observer will be compared to the (regular) EKF for which the parameters have been identified offline. For online parameter estimation (or frequently referred to as parameter adaptation), a wide variety of approaches exists in the literature, see [1, 2, 10] and references therein. These approaches can roughly be divided into two categories. The first category consists of approaches that solve the highly coupled joint-estimation problem in one step, for which the joint EKF and related extensions (e.g., sigma-point KF, unscented KF, etcetera) are well-established in the literature and are widely applied, see, e.g., [1, 2, 8]. The second category consists of approaches that solve the estimation problem in two steps, a parameter-estimation step

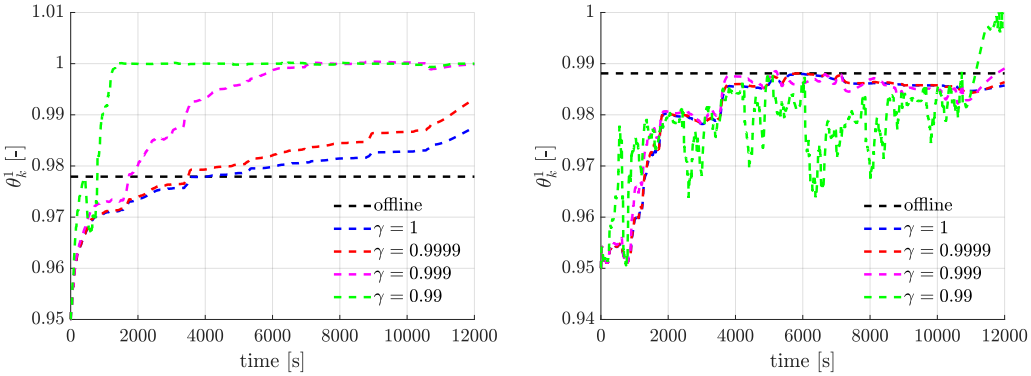

(a) ARX model, θ_k^1.

(b) OE model, θ_k^1.

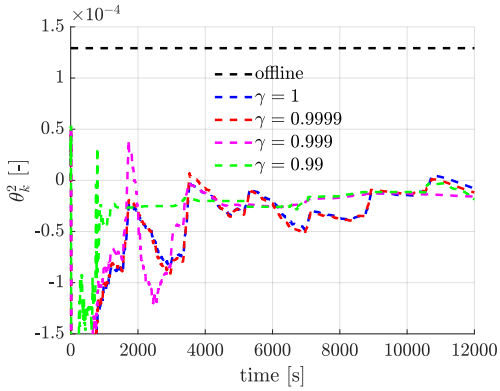

(c) ARX model, θ_k^2.

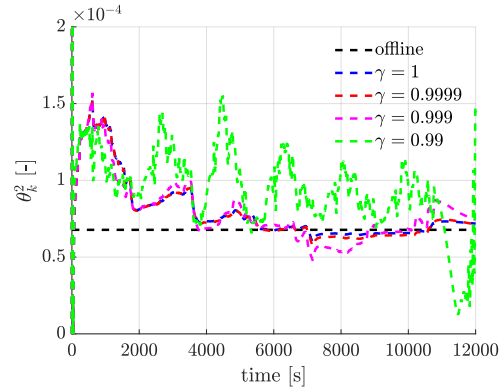

(d) OE model, θ_k^2.

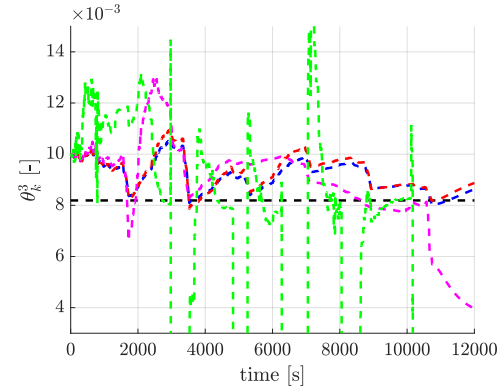

(e) ARX model, θ_k^3.

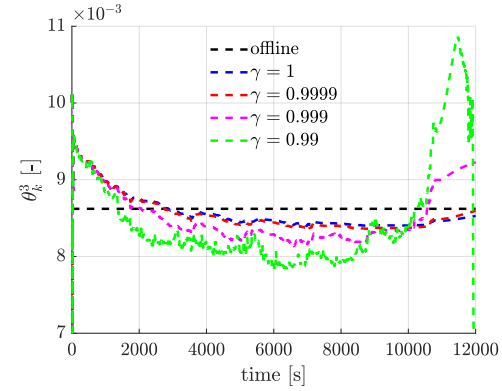

(f) OE model, θ_k^3.

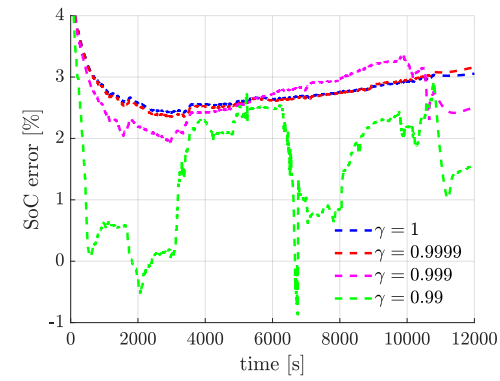

(g) SoC error with ARX model.

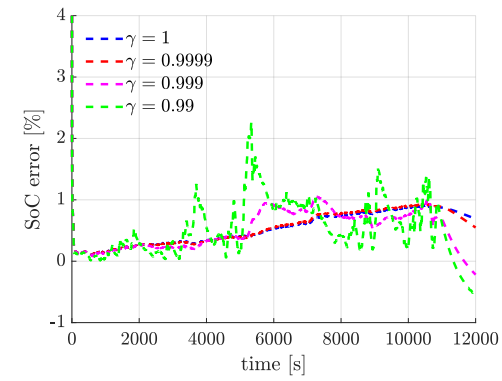

(h) SoC error with OE model.

Fig. 4: Estimated model parameters and SoC error with ARX and OE model for different settings of γ.

and an SoC-estimation step. Typically, the model parameters are estimated using a recursive least-squares (RLS) approach and in the other step, a model (based on the estimated parameters) is used in combination with an EKF for model-based SoC estimation. see, e.g., [27–29]. In summary, the following estimation methods will be compared.

- **Offline EKF:** SoC estimation only; with tuning of (symmetric) covariance matrices $Q \in \mathbb{R}^{2\times 2}$ and $R \in \mathbb{R}^{1\times 1}$ (if a first-order overpotential model is used). No parameter adaptation is employed; the parameters have been identified offline with a separate identification experiment.
- **RLS+EKF:** Two-step approach: parameter estimation using RLS with (a single) forgetting factor γ^{rls} and SoC estimation using an EKF with tuning of (symmetric) covariance matrices $Q \in \mathbb{R}^{2\times 2}$ and $R \in \mathbb{R}^{1\times 1}$.
- **Joint EKF:** Solving the joint-estimation problem using the joint EKF with regular tuning of (symmetric) covariance matrices $Q \in \mathbb{R}^{5\times 5}$ and $R \in \mathbb{R}^{1\times 1}$ (i.e., without correlated noise and forgetting).
- **Joint EKF CF:** The approach developed in this paper based on the joint EKF, with a single tuning parameter γ.

The comparison is performed as follows. The estimation accuracy of the observers is analysed in terms of the SoC estimation error, for which the measured or "true" SoC is calculated with the CC method in combination with the measured current from the lab-grade sensor. The SoC error is then given by subtracting the estimated SoC from the true SoC. The performance of the estimation methods is evaluated for both drive cycles (WLTP and MMD cycle) in Fig. 2 and all observers have been tuned adequately so as to yield good performance (in terms of the SoC estimation error). The offline model parameters (used for the offline EKF and for the initial conditions of the other observers) have been identified with both the MMD and the WLTP cycle. Note that the parameters identified with the MMD cycle are used for the SoC estimation in the WLTP cycle and vice versa, in order to ensure proper cross validation. The initial conditions for the observers are taken as close as possible to the true values, since convergence has already been shown previously in Fig. 4. This means that the initial SoC estimate is taken to be the true SoC and for the joint EKF and the joint EKF CF, the initial conditions for the parameters are taken as the offline identified OE parameters, since in this case, the proposed joint EKF CF uses an OE model structure as discussed in the previous section. Consequently, the other KF-based observers (including the offline EKF) are also initialised with these parameters so as to make a fair comparison. For the two-step scheme with RLS and EKF (RLS+EKF), the initial parameter estimates are the offline identified ARX parameters since an ARX model structure is assumed in the RLS scheme (i.e., only ARX yields a linear least-squares problem). Consequently, the offline parameters have been estimated for both the OE model structure as well as the ARX model structure for both drive cycles. The initial conditions as well as the tuning of the observers are given in Table I.

The results of the comparison can be found in Fig. 5 and Table II. The left column of Fig. 5 depicts the estimation results for the WLTP cycle. The estimated parameters θ_k^1, θ_k^2 and θ_k^3 and the SoC estimation error are shown in Fig. 5 from top to bottom, respectively. As mentioned previously, note that the offline parameters in this figure have been identified with an OE model structure. Similarly, the estimation results for the MMD cycle are depicted in the right column of Fig. 5. Subsequently, the SoC estimation errors in Fig. 5g and Fig. 5h in terms of the root-mean-square error (RMSE) over the entire drive cycle can be found in the third and fourth column of Table II, respectively. The second column of Table II shows the RMSE of the WLTP cycle with the incorrect initial conditions as used in Fig. 4. Furthermore, the baseline for the SoC estimation is shown in Table II by means of the RMSE of the CC method using the production-grade sensor, where the error is mainly caused by the time-varying bias of the production-grade sensor.

In Fig. 5, we can observe that for the WLTP cycle, the performance of the observers is similar and relatively accurate in terms of the SoC estimation error. Table II confirms this as the RMSEs are well below SoC $= 1\%$. For the parameter estimation with the WLTP cycle, the observers behave differently, although the differences in estimated parameters are relatively small. Moreover, the parameter estimates are close to the offline OE model parameters depicted with the dashed magenta line. The results for the MMD cycle in the right column of Fig. 5 are quite similar to those of the WLTP cycle up to $k \approx 9000$s. As mentioned previously, from this point in time (i.e., low SoC range) the battery behaviour becomes more nonlinear, see, e.g., [30]. Therefore, the underlying parameters of the system change, which is clearly visible in the voltage behaviour in Fig. 2f. To deal with this phenomenon, the parameters of the battery model need to be adapted as can be seen in Fig. 5b, Fig. 5d and Fig. 5f, where all observers perform this parameter adaptation differently. The resulting SoC estimation error as well as its RMSE can be found in Fig. 5h and Table II, where it is quite clear that not adapting the parameters, i.e., using the offline EKF, yields the worst performance with an RMSE of 2.7%. This motivates the need to make the parameters of the overpotential model time-varying (e.g., SoC-dependent), thus motivating the need for online parameter estimation. The other observers yield higher accuracy, where the RMSEs for the joint EKF and the proposed joint EKF CF are relatively similar. Note that (for the sake of completeness) the offline EKF has been validated with both OE parameters as well as ARX parameters (the results for the OE parameters are shown in Fig. 5 and Table II). Although the parameter values are slightly different, the estimation accuracy has been found to be the same for both model structures.

TABLE I: Tuning and initial conditions of the observers.

offline EKF	$Q = I_{2\times 2} \times 10^{-4}$, $R = 1$, $P_0 = I_{2\times 2}$
RLS+EKF	$\gamma^{rls} = 0.998$, $P_0^{rls} = I_{3\times 3}$ $Q = I_{2\times 2} \times 10^{-4}$, $R = 1$, $P_0 = I_{2\times 2}$
joint EKF	$Q = I_{5\times 5} \times 10^{-4}$, $R = 1$, $P_0 = I_{5\times 5}$
joint EKF CF	$\gamma = 0.9999$, $P_0 = I_{5\times 5}$

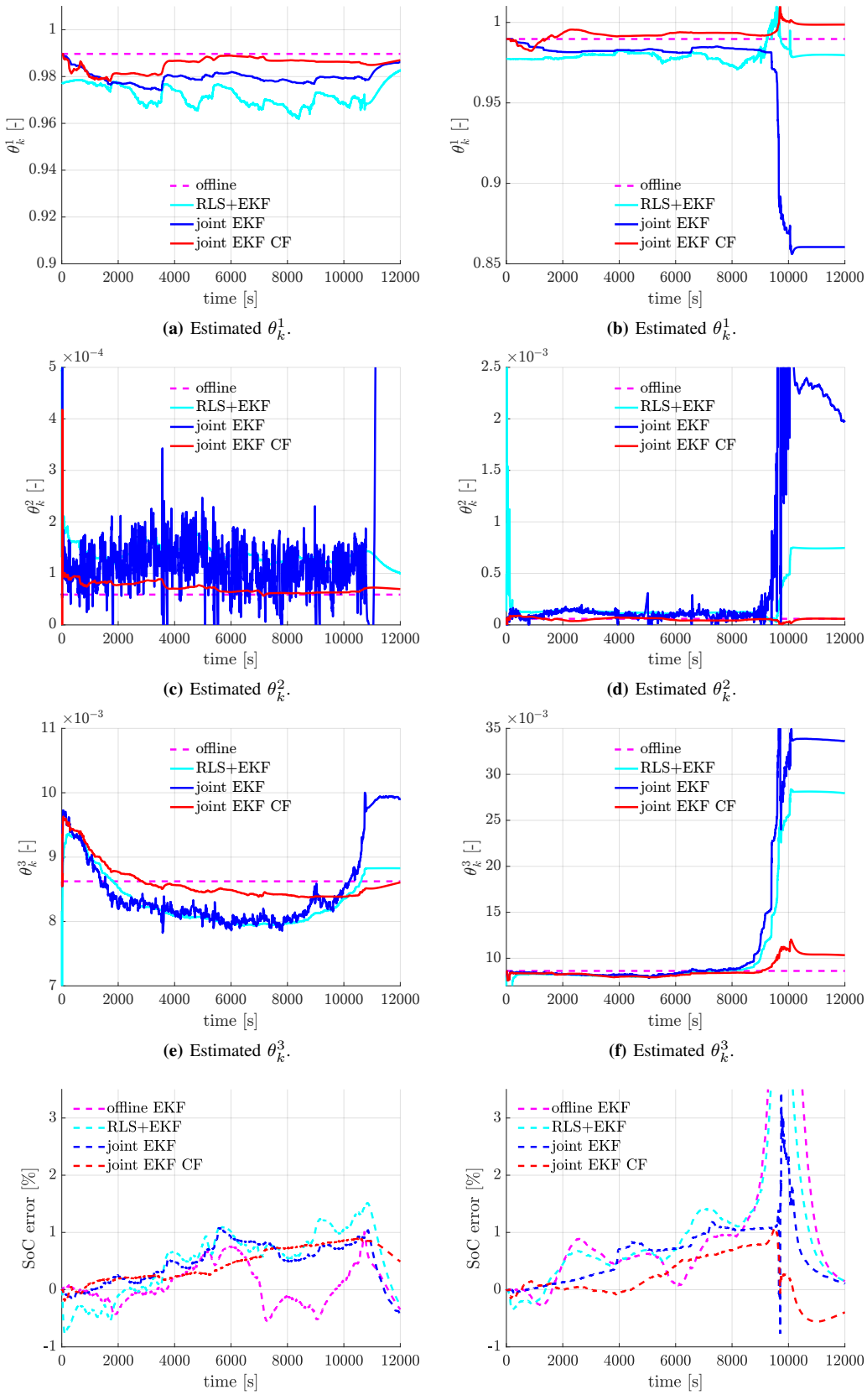

(a) Estimated θ_k^1.

(b) Estimated θ_k^1.

(c) Estimated θ_k^2.

(d) Estimated θ_k^2.

(e) Estimated θ_k^3.

(f) Estimated θ_k^3.

(g) SoC error WLTP cycle.

(h) SoC error MMD cycle.

Fig. 5: Model parameters and SoC error for different observers with in the left column, the results for the WLTP cycle and in the right column, results for the MMD cycle. The offline model parameters have been identified using an OE model structure.

TABLE II: Comparison of the estimation methods in terms of the RMSE of the SoC estimation in [%], including CC (based on the production-grade current sensor) as baseline.

	WLTP (initial error) [%]	WLTP [%]	MMD [%]
CC	5.4	0.5	0.6
offline EKF	0.7	0.4	2.7
RLS+EKF	0.9	0.7	1.7
joint EKF	0.6	0.6	0.8
joint EKF CF	0.6	0.5	0.5

V. Discussion

The results of the application of the proposed observer and the comparison of estimation methods provide interesting insights that are discussed further in this section. First, the proposed joint EKF CF and the (regular) joint EKF achieve similar performance, which is as expected. It is interesting to note that the parameter estimation with the joint EKF seems to be more "aggressive" than with the joint EKF CF, especially for parameters θ_k^2 and θ_k^3 in Fig. 5 as can be seen from the relatively fast parameter variations. In other words, the joint EKF generally works well, but tuning of the observer has been a major issue.

In this paper, the joint EKF has been adapted to make it tuning-friendly with a particular emphasis on disturbance attenuation and convergence properties for SoC estimation. Furthermore, both the joint EKF and the joint EKF CF were able to achieve accurate SoC estimation at the end of the MMD cycle in Fig. 5h, where the nonlinear behaviour of the battery is more pronounced, causing changes in the battery parameters. This demonstrates the advantage of jointly performing SoC and parameter estimation, even though both joint EKFs have slightly higher computational complexity than the offline EKF. It should be noted that both EKFs have similar computational complexity as they have the same state dimensions and require very similar computational operations. Moreover, since both EKFs are capable of adapting the model parameters, they are also both capable of working at different temperatures as temperature has a significant effect on the overpotential of the battery (and thus the value of the model parameters).

Interestingly, the RLS+EKF scheme with the tuning as shown in Table I, which is also a joint-estimation scheme, is significantly less accurate at the end of the MMD cycle. It should be noted that different tuning settings have been analysed for this observer and that the settings as presented in Table I yielded the most accurate results as shown in Table II and Fig. 5h. It would therefore be interesting to further investigate this difference in performance, which might be due to the fact that the joint EKF solves the joint-estimation problem in a strongly coupled fashion, where both the SoC and the parameters are estimated simultaneously, whereas the RLS+EKF scheme uses a more decoupled two-step approach.

Another important aspect is the interpretation of the SoC-estimation results as presented in Table II, Fig. 5g and Fig. 5h. Namely, the RMSEs of the proposed joint EKF CF and the joint EKF are well below 1% SoC error for both drive cycles. However, what does this number tell us and should we aim for an even smaller error, and if so, would that be a significant result? One could argue that an uncertainty interval for the SoC estimation error should be used since the final result, the SoC estimate, consists of a number of steps and each single step introduces some uncertainty. For example, in this paper, the nonlinear EMF-SoC function of the battery model has been characterised at 20°C using a pulsed-current test, which is based on relaxation of the battery voltage. The experimental validation has also been conducted at this temperature. However, the EMF-SoC function is temperature-dependent, see, e.g., [31], which suggests that, depending on the characterisation of the EMF-SoC function, an error in the SoC estimation will be introduced. For example, the function can be characterised as a temperature-dependent function, see, e.g., [9, Chapter 2], or simply as one single curve at one temperature, which is typically used in the literature, see, e.g., [32, Chapter 7]. Still, for the former case, it might be interesting to extend the models used in this paper by including thermal behaviour of the battery and apply the proposed EKF.

Furthermore, the EMF-SoC relation will (slowly) change over time due the battery ageing, see, e.g., [31]. The experiments in this paper are conducted over a short period of time and, therefore, it is assumed that the ageing does not significantly affect the EMF-SoC relation. However, over a longer period of time, the change in the EMF-SoC relation may introduce an additional error in the SoC estimation. Consequently, it is preferable to calibrate or adapt the EMF-SoC relation over time, for which approaches have been proposed, see, e.g., [33, 34], or to incorporate an ageing model in the methodology. Moreover, the method of obtaining the EMF voltage can also introduce an error. For example, using the voltage relaxation method (with the pulsed-current test) is more accurate than using a method where the EMF-SoC curve is determined based on averaging a small discharge current and a small charge current, see [31]. In conclusion, an uncertainty interval around the SoC error of approximately $\pm 1\%$ could very well be reasonable. This would imply that all SoC errors in this interval can be interpreted as equally accurate and we cannot quantitatively compare methods with SoC errors that lie within this interval.

Lastly, one could argue that the RMSE of CC in Table II is relatively small and it could be argued that using an observer for SoC estimation is not necessary. Indeed, for the relatively short drive cycles in this paper, this may be true. However, the problem of the CC method is that it is based on integrating current and therefore the error will accumulate over time. Moreover, and this may be an even bigger issue, the CC method is based on exact knowledge of the initial condition. For instance, using the experimental setup, an experiment of a return trip with the MMD cycle has been performed (i.e., two times 232km) with constant-current charging in between trips. Then, the accumulated SoC error of the correctly initialised CC method (using the production-grade current sensor) was already 4.9% at the end of the cycle, demonstrating the need for SoC estimation. Finally, further drift of the CC accuracy may be caused by battery ageing and self discharge (which are both temperature-dependent phenomena).

VI. Conclusions

Battery State-of-Charge (SoC) estimation is often performed using an nonlinear extension of the Kalman filter such as the Extended Kalman filter (EKF) in combination with an Equivalent-Circuit Model (ECM). However, the convergence of the SoC estimation error and the robustness with respect to model uncertainty are not addressed explicitly, making tuning of these filters a tedious task without clear instructions on the tuning procedure. In the literature, robust-observer design procedures have been proposed that show promising results. However, in order to ensure accurate SoC estimation under all circumstances, joint estimation of SoC and ECM parameters is necessary.

In this paper, it has been shown that extending the robust-observer approaches towards the joint estimation of SoC and ECM parameters is not feasible. Therefore, we have proposed to combine a nonlinear observer with the structured representation of model uncertainty and disturbance as typically used in robust-observer design. To do so, the standard joint EKF has been adapted to accommodate correlated noise and forgetting, which resulted in an observer with a specific structure for model uncertainty and disturbance with a single tuning parameter, allowing for straightforward observer tuning. The experimental results on realistic drive-cycle data have shown that the performance of the proposed observer is similar to the widely-used (and close-to-optimal) joint EKF with a root-mean-square SoC error of 0.5%, resulting in an easy-to-tune alternative to the joint EKF.

Appendix
Implementation of the Forgetting Factor

Using the approach in [26, Chapter 7.4] as a starting point, we will add a forgetting factor to (15) by redefining the covariance matrices in (15) to $Q_k = \gamma^k Q_k$, $R_k = \gamma^k R_k$ and $S_k = \gamma^k S_k$ and by defining $\tilde{P}_k^+ = \gamma^{1-k} P_k^+$ and $\tilde{P}_{k+1}^- = \gamma^{-k} P_{k+1}^-$ in which $\gamma \leq 1$ is the forgetting factor.

The measurement update of the observer is then given by

$$\hat{x}_{k+1}^- = \hat{x}_k^+ + L_k(y_k - C_k\hat{x}_k^+ - D_k u_k) \tag{25}$$

with

$$\begin{aligned} L_k &= P_k^+ C_k^\top \left(C_k P_k^+ C_k^\top + \gamma^k R_k\right)^{-1} \\ &= \gamma^{1-k} P_k^+ C_k^\top \left(\gamma^{1-k} C_k P_k^+ C_k^\top + \gamma^{k-1}\gamma R_k\right)^{-1} \\ &= \tilde{P}_k^+ C_k^\top \left(C_k \tilde{P}_k^+ C_k^\top + \gamma R_k\right)^{-1}, \end{aligned} \tag{26}$$

and

$$\begin{aligned} P_{k+1}^- &= \left(I - L_k C_k\right) P_k^+ \\ \gamma^k \tilde{P}_{k+1}^- &= \left(I - L_k C_k\right) \gamma^{k-1} \tilde{P}_k^+ \\ \tilde{P}_{k+1}^- &= \gamma^{-1} \left(I - L_k C_k\right) \tilde{P}_k^+. \end{aligned} \tag{27}$$

For the time update, we find

$$\begin{aligned} \hat{x}_{k+1}^+ &= A_k\hat{x}_{k+1}^- + B_k u_k + \gamma^k S_k (\gamma^k R_k)^{-1}(y_k - C_k\hat{x}_{k+1}^- - D_k u_k) \\ &= A_k\hat{x}_{k+1}^- + B_k u_k + S_k R_k^{-1}(y_k - C_k\hat{x}_{k+1}^- - D_k u_k) \end{aligned} \tag{28}$$

and

$$\begin{aligned} P_{k+1}^+ &= (A_k - \gamma^k S_k(\gamma^k R_k)^{-1} C_k) P_{k+1}^- \times \\ &\quad (A_k - \gamma^k S_k(\gamma^k R_k)^{-1} C_k)^\top + \gamma^k Q_k - \gamma^k S_k (\gamma^k R_k)^{-1} \gamma^k S_k^\top \\ P_{k+1}^+ &= (A_k - S_k R_k^{-1} C_k) P_{k+1}^- (A_k - S_k R_k^{-1} C_k)^\top \\ &\quad + \gamma^k Q_k - \gamma^k S_k R_k^{-1} S_k^\top \\ \tilde{P}_{k+1}^+ &= (A_k - S_k R_k^{-1} C_k) \tilde{P}_{k+1}^- (A_k - S_k R_k^{-1} C_k)^\top \\ &\quad + Q_k - S_k R_k^{-1} S_k^\top \end{aligned} \tag{29}$$

where $\tilde{P}_{k+1}^+ = \gamma^{-k} P_{k+1}^+$.

In summary, the two-step KF with cross-correlated noise and forgetting is given by the measurement update

$$L_k = \tilde{P}_k^+ C_k^\top (C_k \tilde{P}_k^+ C_k^\top + \gamma R_k)^{-1} \tag{30a}$$

$$\hat{x}_{k+1}^- = \hat{x}_k^+ + L_k(y_k - C_k\hat{x}_k^+ - D_k u_k) \tag{30b}$$

$$\tilde{P}_{k+1}^- = \tfrac{1}{\gamma}(I - L_k C)\tilde{P}_k^+ \tag{30c}$$

and the time update

$$\hat{x}_{k+1}^+ = A_k\hat{x}_{k+1}^- + B_k u_k + S_k R_k^{-1}(y_k - C_k\hat{x}_{k+1}^- - D_k u_k) \tag{30d}$$

$$\begin{aligned} \tilde{P}_{k+1}^+ &= (A_k - S_k R_k^{-1} C) \tilde{P}_{k+1}^- (A_k - S_k R_k^{-1} C)^\top \\ &\quad + Q_k - S_k R_k^{-1} S_k^\top, \end{aligned} \tag{30e}$$

which completes the implementation of the forgetting factor γ.

Acknowledgement

The authors would like to thank our colleagues Prof. Paul Van den Hof for his valuable comments on a draft version of this paper, Will Hendrix for his support in constructing the laboratory test environment, and the anonymous reviewers for their comments and suggestions.

References

[1] Y. Wang, H. Fang, L. Zhou, and T. Wada, "Revisiting the State-of-Charge Estimation for Lithium-Ion Batteries," *IEEE Control Systems Magazine*, vol. 37, no. 4, pp. 73–96, 2017.

[2] R. Xiong, J. Cao, Q. Yu, H. He, and F. Sun, "Critical Review on the Battery State of Charge Estimation Methods for Electric Vehicles," *IEEE Access*, vol. 6, pp. 1832–1843, 2017.

[3] S. Dey, B. Ayalew, and P. Pisu, "Nonlinear Robust Observers for State-of-Charge Estimation of Lithium-Ion Cells Based on a Reduced Electrochemical Model," *IEEE Transactions on Control Systems Technology*, vol. 23, no. 5, pp. 1935–1942, 2015.

[4] P. G. Blondel and R. Postoyan, "Observer design for an electrochemical model of lithium ion batteries based on a polytopic approach," in *Proc. IFAC World Congress*, 2017, pp. 8457–8462.

[5] H. P. G. J. Beelen, H. J. Bergveld, and M. C. F. Donkers, "On Experiment Design for Parameter Estimation of Equivalent-Circuit Battery Models," in *Proc. IEEE Conf. on Control Technology and Applications*, 2018, pp. 1526–1531.

[6] A. Klintberg, T. Wik, and B. Fridholm, "Theoretical Bounds on the Accuracy of State and Parameter Estimation for Batteries," in *Proc. American Control Conf.*, 2017, pp. 4035–4041.

[7] C. Campestrini, T. Heil, S. Kosch, and A. Jossen, "A comparative study and review of different Kalman filters by applying an enhanced validation method," *Journal of Energy Storage*, vol. 8, pp. 142–159, 2016.

[8] G. L. Plett, "Extended Kalman filtering for battery management systems of LiPB-based HEV battery packs; Part 3. State and parameter estimation," *Journal of Power Sources*, vol. 134, no. 2, pp. 277–292, 2004.

[9] ——, *Battery Management Systems: Equivalent-Circuit Methods*, 1st ed. Artech House, 2016.

[10] M. U. Cuma and T. Koroglu, "A comprehensive review on estimation strategies used in hybrid and battery electric vehicles," *Renewable and Sustainable Energy Reviews*, vol. 42, pp. 517–531, 2015.

[11] K. Reif, S. Günther, E. Yaz, and R. Unbehauen, "Stochastic stability of the discrete-time extended Kalman filter," *IEEE Transactions on Automatic Control*, vol. 44, no. 4, pp. 714–728, 1999.

[12] M. Boutayeb, H. Rafaralahy, and M. Darouach, "Convergence analysis of the extended Kalman filter as an observer for nonlinear discrete-time systems," *IEEE Transactions on Automatic Control*, vol. 42, no. 4, pp. 581–586, 1997.

[13] L. Ljung, "Asymptotic Behavior of the Extended Kalman Filter as a Parameter Estimator for Linear Systems," *IEEE Transactions on Automatic Control*, vol. 24, no. 1, pp. 36–50, 1979.

[14] B. Fridholm, M. Nilsson, and T. Wik, "Robustness comparison of battery state of charge observers for automotive applications," in *Proc. IFAC World Congress*, 2014, pp. 2138–2146.

[15] X. Lin, "Theoretical Analysis of Battery SOC Estimation Errors under Sensor Bias and Variance," *IEEE Transactions on Industrial Electronics*, vol. 65, no. 9, pp. 7138–7148, 2018.

[16] H. J. Dreef, H. P. G. J. Beelen, and M. C. F. Donkers, "LMI-based Robust Observer Design for Battery State-of-Charge Estimation," in *Proc. IEEE Conf. on Decision and Control*, 2018, pp. 5716–5721.

[17] S. Bezzaoucha, B. Marx, D. Maquin, and J. Ragot, "State and parameter estimation for time-varying systems: a Takagi-Sugeno approach," in *Proc. IFAC Symposium on System Structure and Control*, 2013, pp. 761–766.

[18] X. Hu, S. Li, and H. Peng, "A comparative study of equivalent circuit models for Li-ion batteries," *Journal of Power Sources*, vol. 198, pp. 359–367, 2012.

[19] L. Ljung, *System Identification: Theory for the User*, 2nd ed. Prentice Hall, 1999.

[20] A. Farmann, W. Waag, A. Marongiu, and D. U. Sauer, "Critical review of on-board capacity estimation techniques for lithium-ion batteries in electric and hybrid electric vehicles," *Journal of Power Sources*, vol. 281, pp. 114–130, 2015.

[21] S. Zhao, S. R. Duncan, and D. A. Howey, "Observability Analysis and State Estimation of Lithium-Ion Batteries in the Presence of Sensor Biases," *IEEE Transactions on Control Systems Technology*, vol. 25, no. 1, pp. 326 – 333, 2017.

[22] L. Zhao, Z. Liu, and G. Ji, "Lithium-ion battery state of charge estimation with model parameters adaptation using H-infinity extended Kalman filter," *Control Engineering Practice*, vol. 81, pp. 114–128, 2018.

[23] J. Schorsch, L. D. Couto, and M. Kinnaert, "SOC and SOH estimation for Li-ion battery based on an equivalent hydraulic model. Part I: SOC and surface concentration estimation," in *Proc. American Control Conf.*, 2016, pp. 4022–4028.

[24] X. Lin, "A Data Selection Strategy for Real-time Estimation of Battery Parameters," in *Proc. American Control Conf.*, 2018, pp. 2276–2281.

[25] B. D. O. Anderson and J. B. Moore, *Optimal Filtering*, 1st ed. Prentice-Hall, 1979.

[26] D. Simon, *Optimal State Estimation: Kalman, H-infinity, and Nonlinear Approaches*, 1st ed. John Wiley & Sons, 2006.

[27] F. Baronti, R. Roncella, R. Saletti, and W. Zamboni, "FPGA implementation of the mix algorithm for state-of-charge estimation of Lithium-ion batteries," in *Proc. IEEE Industrial Electronics Conf.*, 2014, pp. 5641–5646.

[28] F. Codeca, S. M. Savaresi, and G. Rizzoni, "On battery State of Charge estimation: A new mixed algorithm," in *Proc. IEEE Conf. on Control Applications*, 2008, pp. 102–107.

[29] R. Xiong, F. Sun, H. He, and T. D. Nguyen, "A data-driven based adaptive state of charge estimator of lithium-ion polymer battery used in electric vehicles," *Applied Energy*, vol. 113, pp. 1421–1433, 2014.

[30] R. Relan, Y. Firouz, J.-M. Timmermans, and J. Schoukens, "Data-Driven Nonlinear Identification of Li-Ion Battery Based on a Frequency Domain Nonparametric Analysis," *IEEE Transactions on Control Systems Technology*, vol. 25, no. 5, pp. 1825–1832, 2017.

[31] V. Pop, H. J. Bergveld, D. Danilov, P. P. L. Regtien, and P. H. L. Notten, *Battery Management Systems: Accurate State-of-Charge Indication for Battery-Powered Applications*, 1st ed. Springer Science + Business Media, 2008.

[32] H. P. G. J. Beelen, "Model-Based Temperature and State-of-Charge Estimation for Li-ion Batteries," Dissertation, Eindhoven University of Technology, 2019.

[33] A. Klintberg, E. Klintberg, B. Fridholm, H. Kuusisto, and T. Wik, "Statistical modeling of OCV-curves for aged battery cells," in *Proc. IFAC World Congress*, 2017, pp. 2164–2168.

[34] A. Klintberg, C. Zou, B. Fridholm, and T. Wik, "Kalman filter for adaptive learning of two-dimensional look-up tables applied to OCV-curves for aged battery cells," *Control Engineering Practice*, vol. 84, pp. 230–237, 2019.